ELSEVIER

Contents lists available at ScienceDirect

#### NeuroImage

journal homepage: www.elsevier.com/locate/neuroimage



# Sex differences in network controllability as a predictor of executive function in youth



Eli J. Cornblath <sup>a,b</sup>, Evelyn Tang <sup>b</sup>, Graham L. Baum <sup>a,b,c</sup>, Tyler M. Moore <sup>c</sup>, Azeez Adebimpe <sup>c</sup>, David R. Roalf <sup>c</sup>, Ruben C. Gur <sup>c</sup>, Raquel E. Gur <sup>c</sup>, Fabio Pasqualetti <sup>d</sup>, Theodore D. Satterthwaite <sup>c,1</sup>, Danielle S. Bassett <sup>b,e,f,g,\*,1</sup>

- <sup>a</sup> Department of Neuroscience, Perelman School of Medicine, University of Pennsylvania, Philadelphia, PA, 19104, USA
- b Department of Bioengineering, School of Engineering and Applied Sciences, University of Pennsylvania, Philadelphia, PA, 19104, USA
- <sup>c</sup> Department of Psychiatry, Perelman School of Medicine, University of Pennsylvania, Philadelphia, PA, 19104, USA
- <sup>d</sup> Department of Mechanical Engineering, University of California, Riverside, CA, 92521, USA
- e Department of Physics & Astronomy, College of Arts and Sciences, University of Pennsylvania, Philadelphia, PA, 19104, USA
- f Department of Neurology, Perelman School of Medicine, University of Pennsylvania, Philadelphia, PA, 19104, USA
- g Department of Electrical and Systems Engineering, School of Engineering and Applied Sciences, University of Pennsylvania, Philadelphia, PA, 19104, USA

#### ARTICLE INFO

# Keywords: Network controllability Neurodevelopment Sex differences Executive function Working memory fMRI BOLD Diffusion tensor imaging

#### ABSTRACT

Executive function is a quintessential human capacity that emerges late in development and displays different developmental trends in males and females. Sex differences in executive function in youth have been linked to vulnerability to psychopathology as well as to behaviors that impinge on health, wellbeing, and longevity. Yet, the neurobiological basis of these differences is not well understood, in part due to the spatiotemporal complexity inherent in patterns of brain network maturation supporting executive function. Here we test the hypothesis that sex differences in impulsivity in youth stem from sex differences in the controllability of structural brain networks as they rewire over development. Combining methods from network neuroscience and network control theory, we characterize the network control properties of structural brain networks estimated from diffusion imaging data acquired in males and females in a sample of 879 youth aged 8-22 years. We summarize the control properties of these networks by estimating average and modal controllability, two statistics that probe the ease with which brain areas can drive the network towards easy versus difficult-to-reach states. We find that females have higher modal controllability in frontal, parietal, and subcortical regions while males have higher average controllability in frontal and subcortical regions. Furthermore, controllability profiles in males are negatively related to the false positive rate on a continuous performance task, a common measure of impulsivity. Finally, we find associations between average controllability and individual differences in activation during an n-back working memory task. Taken together, our findings support the notion that sex differences in the controllability of structural brain networks can partially explain sex differences in executive function. Controllability of structural brain networks also predicts features of task-relevant activation, suggesting the potential for controllability to represent contextspecific constraints on network state more generally.

#### 1. Introduction

Executive function is necessary for regulation of goal-directed behavior, and encompasses cognitive processes including working memory, sustained attention, inhibition, task switching, and performance monitoring (Anderson et al., 2001). Deficits in the various subdomains of executive function can greatly hinder quality of life. For example, deficits in sustained attention can hamper academic and occupational performance (Biederman et al., 2007) while impulsivity can lead to increased risk taking and associated consequences (Romer et al., 2009; Barkley et al., 2002; Cross et al., 2011; Weafer and de Wit, 2014). While many investigations of sex differences are limited by small sample sizes (Hyde, 2014), biopsychosocial confounds (Miller and Halpern, 2014), and a focus on sex assigned at birth (Joel, 2012), meta analysis

<sup>\*</sup> Corresponding author. Department of Bioengineering, School of Engineering and Applied Sciences, University of Pennsylvania, Philadelphia, PA, 19104, USA. *E-mail address*: dsb@seas.upenn.edu (D.S. Bassett).

<sup>&</sup>lt;sup>1</sup> These authors contributed equally to this work.

(Hasson and Fine, 2012) and large studies (Gur et al., 2012; Riley et al., 2016) suggest that within the executive function domain, males exhibit selective dysfunction in impulsivity relative to their female counterparts, as measured by commission error, or false positives, on the continuous performance task (CPT). Accordingly, these selective executive deficits may underlie the higher rates of criminality (Cross et al., 2011), violence (Cross et al., 2011), and substance use initiation (Romer et al., 2009; Cross et al., 2011; Weafer and de Wit, 2014) among males. Current interventions for disorders of executive function usually do not consider sex and are relatively limited to psychotherapy and non-specific psychopharmacology (Hosenbocus and Chahal, 2012). It remains unknown whether and to what extent the pathophysiology of executive deficits is sex-specific. Thus, investigating sex differences in the neurobiology supporting executive function can be a powerful tool for revealing clinically relevant variation, with potential applications for developing personalized interventions for neuropsychiatric illness.

A basic understanding of sex-related differences in executive function and their implications for the diagnosis and treatment of executive deficits requires an understanding of the normative maturation of underlying neural circuitry. Several studies highlight the fact that such maturation, and sex differences in that maturation, span structure (Gogtay et al., 2004), anatomical connectivity (Baum et al., 2017), activity (Schmithorst et al., 2015; Nomi et al., 2017; Keulers et al., 2011), and functional connectivity (Fair et al., 2009). Using structural MRI, a recent study (Gennatas et al., 2017) reported age-related, non-linear increases in gray matter density with concurrent decreases in cortical thickness. Interestingly, the maturation of these structural features was markedly different between the sexes, with females showing higher gray matter density globally and higher cortical thickness in frontal and insular regions (Gennatas et al., 2017). Using diffusion-weighted MRI, another study found significantly greater within-hemisphere connectivity in males and greater between-hemisphere connectivity in females (Ingalhalikar et al., 2014). Sex differences have also been identified in the clustered (or modular) structure in patterns of functional connectivity estimated from resting state fMRI data: males display higher between-module connectivity while females display higher within-module connectivity (Satterthwaite et al., 2014a). Despite these important descriptive studies, it remains difficult to specify in a mechanistic sense how executive function might arise from such complex, multimodal patterns of brain maturation influenced by biological sex.

We posit that such a mechanistic understanding could emerge from recent advances in *network control theory*, an emerging branch of theoretical physics and systems engineering that models how network dynamics can be predictably influenced (Liu et al., 2011; Pasqualetti et al., 2014; Kailath, 1980; Kalman et al., 1963) (Fig. 1). Prior work has demonstrated the utility of network control theory in understanding basic brain

architecture and function (Muldoon et al., 2016; Betzel et al., 2016; Gu et al., 2017) across spatial scales (Wiles et al., 2017) and species (Kim et al., 2018), posited its relation to cognition (Gu et al., 2015; Tang et al., 2017) and psychiatric illness (Jeganathan et al., 2018), and outlined its developmental timecourse (Tang et al., 2017). Intuitively, the control of brain dynamics instantiated in the notion of network controllability could prove relevant for the control of behavior as instantiated in the notion of impulse control, a key component of executive function (Diamond, 2013). In response to environmental demands, white matter connectivity must allow for transitions to states of brain activity supporting cognition and behavior (Betzel et al., 2016; Gu et al., 2017; Cornblath et al., 2018). Control properties therefore impact a system's possible trajectories through different states of activity, as well as the manner in which the system responds to external stimuli (Gu et al., 2017).

We hypothesize that sex differences in impulse control in youth stem from sex differences in the controllability of structural brain networks as they rewire over development. Sex differences in control properties could manifest in a reduced ability of some youths, especially males, to reach states that support robust impulse control, or they could result in an increased propensity to occupy states that are unfavorable for impulse control. Thus, we did not make any directional hypotheses regarding the effects of increasing network controllability. Accordingly, we focused on identifying control points whose regional input can be used to drive state transitions in a linear system. Control points are identified with metrics that assess the ability of specific nodes to alter the state of the system, based on the underlying network topology and a specification of network dynamics (Pasqualetti et al., 2014) (Fig. 1). The metric of average controllability reflects the average energy input required at a node to move the system from some initial state to all possible states (Gu et al., 2015; Tang et al., 2017; Jeganathan et al., 2018). In contrast, the metric of modal controllability reflects the ease of transitioning the system from some initial state to a difficult-to-reach state (Pasqualetti et al., 2014; Gu et al., 2015; Tang et al., 2017).

Hence, we move forward by describing sex differences in network controllability using the metrics of average and modal controllability, and measuring impulse control using the false positive rate on the CPT (Gur et al., 2010). Specifically, we predicted that (i) network controllability differs by sex, (ii) network controllability changes with age differently in males and females, (iii) sex differences in network controllability predict false positives on the CPT (Gur et al., 2010), and (iv) network controllability predicts the activation of brain regions during a working memory task demanding executive function. To test these predictions, we constructed structural brain networks from diffusion tensor imaging data acquired in 879 healthy youth, ages 8–22 years, in the Philadelphia Neurodevelopmental Cohort (PNC) (Satterthwaite et al.,

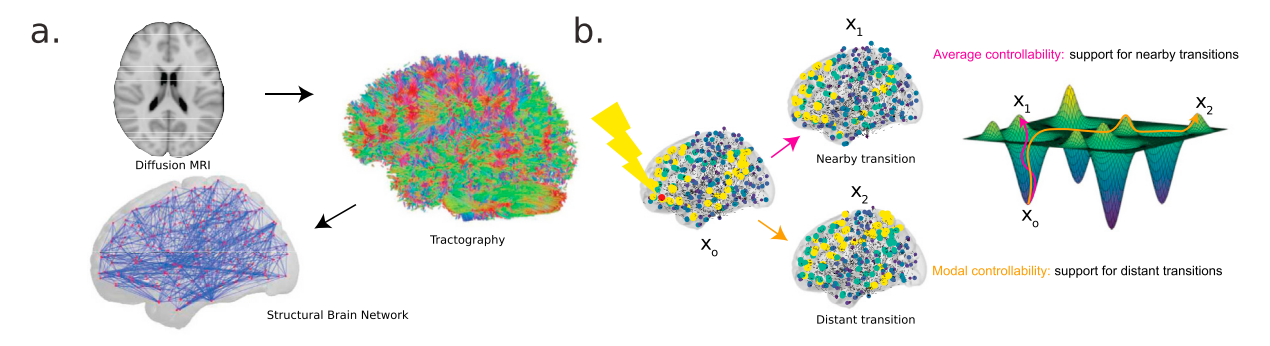


Fig. 1. Control theory and schematic of data processing. (a) Schematic depicting the basic methodological approach. Diffusion tensor imaging (DTI) data was acquired from 879 youth between the age of 8 years and 22 years. Deterministic tractography was used to identify the number of white matter streamlines, connecting any two regions of interest. These estimates were used to construct a structural brain network for each subject representing white matter connectivity (edges) between brain regions (nodes). (b) Schematic (right) of a state space of a two-dimensional dynamical system where the z-value and color indicate some energetic cost associated with occupying a particular pair of x-y coordinates, alongside a diagram (left) illustrating brain state transitions from an activated default mode system ( $\mathbf{x}_0$ ). The blue arrow denotes a distant transition to a deactivated default mode system and activated frontoparietal/dorsal attention system ( $\mathbf{x}_2$ ). The red arrow denotes a nearby transition to a partially deactivated default mode system ( $\mathbf{x}_1$ ). Regions with high modal controllability can facilitate transitions to energetically distant states while regions with high average controllability can facilitate transitions to nearby states while requiring very little energy.

2014b). Each brain network was comprised of 234 anatomically defined regions (Cammoun et al., 2012) connected by white matter tracts estimated from diffusion tractography. We show that regional controllability is a significant mediator of the relationship between sex and impulse control, and that it predicts the magnitude of fMRI BOLD signal on an n-back task, a brain state associated with high demands on working memory, a separate domain of executive function. As described in detail below, our results suggest that sex differences in the controllability of structural brain networks predict impulse control and that network control properties explain the activity profiles that support executive function more broadly.

#### 2. Materials and methods

#### 2.1. Participants

Diffusion tensor imaging (DTI) data were obtained from youth who participated in a large community-based study of brain development, now known as the Philadelphia Neurodevelopmental Cohort (PNC) (Satterthwaite et al., 2014b). Here we study 879 out of a total of 1601 subjects between the ages of 8 and 22 years. Due to lack of complete diffusion scans (n = 227) and incidental findings (n = 20), data from 244 participants was deemed unusable. The remaining 1354 participants underwent a rigorous manual and automated quality assurance protocol for DTI datasets (Roalf et al., 2016), eliminating an additional 147 subjects with poor data quality. A subset of 93 of the remaining 1207 participants were excluded for low quality or incomplete FreeSurfer reconstruction of T1-weighted images (Rosen et al., 2018). Further, 235 of the remaining 1114 participants were excluded for one or more of the following reasons: gross radiological abnormalities distorting brain anatomy, medical history that might impact brain function, history of inpatient psychiatric hospitalization, use of psychotropic medication at the time of imaging, or high levels of in-scanner head motion during the DTI scan, as defined by a mean relative displacement between non-weighted volumes of greater than 2 mm. These exclusions left us with a final sample of n = 879 subjects (Baum et al., 2017; Tang et al., 2017) between the ages of 8 and 22 years (mean age = 15.06, SD = 3.15; 389 males, 490 females).

	Males	Females
Age (y)	$15\pm3.2$	$15.1\pm3.1$
White	48.6%	37.8%
African American	39.3%	50.2%
Other Race	12.1%	12.0%
d' (n-back)	$1.94\pm0.75$	$1.87\pm0.73$
CPT False Positives (z)	$-0.131 \pm 0.72$	$-0.324 \pm 0.71$

#### 2.2. Cognitive phenotyping

Cognition was measured outside of the scanner using the Penn Computerized Neurocognitive Battery (CNB) (Gur et al., 2010, 2012). Briefly, the 1-hour CNB was administered to all participants, and consisted of 14 tests that evaluated a broad range of cognitive functions. Twelve of the tests measure both accuracy and speed, while two of the tests (motor and sensorimotor) measure only speed.

In this study, we focus our analysis of executive function on the continuous performance task (CPT). During the CPT, the participant is presented with 7-segment displays of vertical and horizontal lines (at a rate of one display per second), and the participant must press a button when the lines form a number (first 1.5 minutes) or a letter (second 1.5 minutes) (Gur et al., 2010). This task measures sustained attention via the true positive rate, and it measures impulsivity via the false positive rate (Gur et al., 2010). A previous study (Gur et al., 2012) that administered the CPT via the Penn CNB (Gur et al., 2010) found a higher true

positive rate in females, while other measures of executive function such as working memory did not exhibit sex differences. In our sample, we observed no significant difference in CPT true positive rate between males and females. However, the CPT false positive rate on the same task was higher in males, consistent with a sex difference in impulse control. Because impulse control intuitively relies on the coordination of spatially distributed brain networks (Brewer and Potenza, 2008), we focus the cognitive portion of the present analysis on CPT false positives. Of note, 10 subjects in our sample had missing data for the CPT and thus were excluded from analyses involving CPT data (Figs. 6 and 7).

#### 2.3. Imaging data acquisition

MRI data were acquired on a 3 Tesla Siemens Tim Trio whole-body scanner and 32-channel head coil at the Hospital of the University of Pennsylvania. DTI scans were acquired via a twice-refocused spin-echo (TRSE) single-shot echo-planar imaging (EPI) sequence (TR = 8100 ms, TE = 82 ms, FOV =  $240 \, \mathrm{mm}^2/240 \, \mathrm{mm}^2$ ; Matrix = RL:128/AP:128/Slices:70, in-plane resolution (x and y) 1.875 mm²; slice thickness = 2 mm, gap = 0; flip angle =  $90/180/180^\circ$ , volumes = 71, GRAPPA factor = 3, bandwidth =  $2170 \, \mathrm{Hz/pixel}$ , PE direction = AP). This sequence utilizes a four-lobed diffusion encoding gradient scheme combined with a 90-180-180 spin-echo sequence designed to minimize eddy-current artifacts. The complete sequence consisted of 64 diffusion-weighted directions with  $b = 1000 \, \mathrm{s/mm}^2$  and 7 interspersed scans where  $b = 0 \, \mathrm{s/mm}^2$ . Total scan time was approximately 11 min. The imaging volume was prescribed in axial orientation covering the entire cerebrum with the topmost slice being located just superior to the apex of the brain.

In addition to the DTI scan, a B0 map of the main magnetic field was derived from a double-echo, gradient-recalled echo (GRE) sequence, allowing us to estimate field distortions in each dataset. Prior to DTI acquisition, a 5-min magnetization-prepared, rapid acquisition gradientecho T1-weighted (MPRAGE) image (TR 1810 ms, TE 3.51 ms, FOV 180  $\times$  240 mm, matrix 256  $\times$  192, effective voxel resolution of 1  $\times$  1  $\times$ 1 mm) was acquired. This high-resolution structural image was used for tissue segmentation and parcellating gray matter into anatomically defined regions in native space. Rigorous manual and automated quality assurance protocols for the T1-weighted structural imaging data were performed for the 879 subjects considered here (Vandekar et al., 2015). Subsequently, all structural images were processed using FreeSurfer (version 5.3) (Fischl, 2012). FreeSurfer reconstructions underwent rigorous quality assurance protocols (Vandekar et al., 2015; Rosen et al., 2018). The T1 image was parcellated into 234 regions by FreeSurfer according to the Lausanne Atlas (Cuadra et al., 2004). We define the subcortex of this 234-region parcellation to be comprised of the left and right hemispheric counterparts of the thalamus proper, caudate, putamen, pallidum, nucleus accumbens area, hippocampus, and amygdala, while excluding the brainstem (14 regions). We define the cortex of this 234-region parcellation to be comprised of the remaining areas (219 regions).

fMRI BOLD data were acquired as subjects completed a version of the n-back working memory task using fractal images (Ragland et al., 2002). See the Ref. (Satterthwaite et al., 2013) for details regarding task presentation and structure. Functional images were obtained using a whole-brain, single-shot, multislice, gradient-echo echoplanar sequence (231 vol; TR = 3000 ms; TE = 32 ms; flip angle = 90 degrees; FOV =  $192 \times 192$  mm; matrix =  $64 \times 64$ ; slices = 46; slice thickness = 3 mm; slice gap = 0 mm; effective voxel resolution =  $3.0 \times 3.0 \times 3.0$  mm).

#### 2.4. Imaging data preprocessing

All DTI datasets were subject to a rigorous manual quality assessment procedure involving visual inspection of all 71 volumes (Roalf et al., 2016). Each volume was evaluated for the presence of artifact, with the total number of volumes that were impacted summed over the series. This scoring was based on previous work describing the impact of

removing image volumes when estimating the diffusion tensor (Jones and Basser, 2004; Chen et al., 2015). Data was considered "Poor" if more than 14 (20%) volumes contained artifact, "Good" if between 1 and 14 volumes contained artifact, and "Excellent" if no visible artifacts were detected in any volumes. All 879 subjects included in the present study had diffusion datasets identified as "Good" or "Excellent," and had less than 2 mm mean relative displacement between interspersed b=0 volumes. As described below, even after this rigorous quality assurance protocol, motion was included as a covariate in all analyses.

The skull was removed for each subject by registering a binary mask of a standard fractional anisotropy (FA) map (FMRIB58 FA) to each subject's DTI image using an affine transformation (Jenkinson et al., 2002). Eddy currents and subject motion were estimated and corrected using the FSL eddy tool (Andersson and Sotiropoulos, 2016). Diffusion gradient vectors were then rotated to adjust for subject motion estimated by eddy. After the field map was estimated, distortion correction was applied to DTI data using FSL's FUGUE (Jenkinson et al., 2012).

BOLD time series were processed as described in (Satterthwaite et al., 2013; Shanmugan et al., 2016). Briefly, FSL 5 (Jenkinson et al., 2012) was used to analyze time series data from three condition blocks (0-back, 1-back and 2-back), with the primary contrast being 2-back> 0-back. BOLD images were co-registered to the T1 image using boundary-based registration (Greve and Fischl, 2009) with integrated distortion correction as implemented in FSL. Generalized linear model (GLM) beta weights were averaged across all voxels in each parcel of the 234-node Lausanne atlas. In our assessment of n-back performance-related activation, we use the difference in GLM beta weights between the 2-back and 0-back condition. For all analyses of fMRI data, we excluded 42 subjects with incomplete data or excessive head motion (mean relative displacement > 0.5 mm or maximum displacement > 6 mm), leaving n = 837 remaining.

#### 2.5. Structural network estimation

Structural connectivity was estimated from DTI data in order to generate the adjacency matrix representing the pattern of white matter tracts between large-scale brain areas. DSI Studio was used to estimate the diffusion tensor and perform deterministic whole-brain fiber tracking with a modified FACT algorithm that used exactly 1,000,000 streamlines per subject after removing all streamlines with length < 10 mm (Gu et al., 2015). To extend regions into white matter, parcels defined using the Lausanne atlas were dilated by 4 mm (Gu et al., 2015; Tang et al., 2017) and registered to the first non-weighted (b = 0) volume using an affine transform (Gu et al., 2015; Tang et al., 2017). The number of streamlines connecting node i and node j in the 234-region parcellation was used to weight the edge  $A_{ij}$  of the adjacency matrix  $\bf A$ .

#### 2.6. Network controllability

We represent the streamline-weighted structural network estimated from diffusion tractography as the graph  $\mathscr{G}=(\mathscr{V},\mathscr{E})$ , where  $\mathscr{V}$  and  $\mathscr{E}$  are the vertex and edge sets, respectively. Let  $A_{ij}$  be the weight associated with the edge  $(i,j)\in\mathscr{E}$ , and define the weighted adjacency matrix of  $\mathscr{G}$  as  $A=[A_{ij}]$ , where  $A_{ij}=0$  whenever  $(i,j)\notin\mathscr{E}$ . We associate a real value with each node to generate a vector describing the network state, and we define the map  $x:\mathbb{N}_{\geq 0}\to\mathbb{R}^N$  to describe the dynamics of the network state over time.

It is worth noting that this method assumes that the number of streamlines is proportional to the strength of structural connectivity with regards to propagation of activity between nodes according to a specified model of dynamics. Here we employ a simplified noise-free linear discrete-time and time-invariant model of such dynamics:

$$\mathbf{x}(t+1) = \mathbf{A}\mathbf{x}(t) + \mathbf{B}_{\mathscr{X}}\mathbf{u}_{\mathscr{X}}(t), \tag{1}$$

where x describes the state (i.e. voltage, firing rate, BOLD signal) of brain regions over time. Thus, the state vector x has length N, where N is the

number of brain regions in the parcellation, and the value of  $\mathbf{x}_i$  describes the activity level of that region. The matrix  $\mathbf{A}$  is symmetric, with the diagonal elements satisfying  $A_{ii}=0$ . Prior to calculating controllability values, we divide  $\mathbf{A}$  by  $1+\xi_0(\mathbf{A})$ , where  $\xi_0(\mathbf{A})$  is the largest eigenvalue of  $\mathbf{A}$ . The input matrix  $\mathbf{B}_{\mathscr{X}}$  identifies the control point  $\mathscr{X}$  in the brain, where  $\mathscr{X}=k_1,\ldots,k_m$  and

$$\mathbf{B}_{\mathscr{X}} = [e_{k_1} \cdots e_{k_m}],\tag{2}$$

and  $e_i$  denotes the *i*-th canonical vector of dimension N. The input  $\mathbf{u}_{\mathcal{X}}:\mathbb{R}_{>0}\to\mathbb{R}^M$  denotes the control strategy.

To study the dynamics by which the activity of one brain region influences structurally connected regions, we apply the control theoretic notion of controllability to our dynamical model. Classic results in control theory ensure that controllability of the network,  $\mathbf{x}(t+1) = \mathbf{A}\mathbf{x}(t) + \mathbf{B}_{\mathscr{K}}\mathbf{u}_{\mathscr{K}}(t)$ , from the set of network nodes  $\mathscr{K}$  is equivalent to the controllability Gramian  $\mathbf{W}_{\mathscr{K}}$  being invertible, where

$$\mathbf{W}_{\mathscr{X}} = \sum_{r=0}^{\infty} \mathbf{A}^{r} \mathbf{B}_{\mathscr{X}} \mathbf{B}_{\mathscr{X}}^{T} \mathbf{A}^{r}. \tag{3}$$

We calculate  $\mathbf{W}_{\mathcal{X}}$ , or rather  $\mathbf{W}_i$ , with  $\mathbf{B}_{\mathcal{X}}$  set equal to one canonical vector  $e_i$  and repeat this process for all N nodes (Gu et al., 2015; Tang et al., 2017). Although it is well known that the activity of several brain regions and neuronal ensembles are related via non-linear dynamics, it has been shown that a linear approximation can explain features of the resting state fMRI BOLD signal (Honey et al., 2009); this suggests that a linear approximation can effectively capture the controllability properties of the original non-linear dynamics.

#### 2.7. Controllability metrics

Following Ref. (Gu et al., 2015; Tang et al., 2017), controllability metrics for structural brain networks were calculated for two different control strategies that describe the ability to change  $\mathbf{x}(t)$  in a particular fashion (Pasqualetti et al., 2014). Average controllability describes the ease of transition to energetically similar states, while modal controllability describes the ease of transition to difficult-to-reach states (Pasqualetti et al., 2014).

Average controllability of a network equals the average input energy applied to a set of control nodes required to reach all possible target states. It is known that average input energy is proportional to  $\operatorname{Trace}(\mathbf{W}_{\mathscr{H}}^{-1})$ , the trace of the inverse of the controllability Gramian. Following Refs. (Gu et al., 2015; Tang et al., 2017), we use  $\operatorname{Trace}(\mathbf{W}_{\mathscr{H}})$  as an alternative measure of average controllability because (i)  $\operatorname{Trace}(\mathbf{W}_{\mathscr{H}})$  and  $\operatorname{Trace}(\mathbf{W}_{\mathscr{H}}^{-1})$  are related via inverse proportionality, and (ii)  $\operatorname{Trace}(\mathbf{W}_{\mathscr{H}}^{-1})$  tends to be very ill-conditioned and cannot be accurately computed even at more coarse connectome parcellations. In addition to its relationship with  $\operatorname{Trace}(\mathbf{W}_{\mathscr{H}}^{-1})$ ,  $\operatorname{Trace}(\mathbf{W}_{\mathscr{H}})$  describes the energy of the network impulse response, or, equivalently, the network  $H_2$  norm (Kailath, 1980; Kalman et al., 1963). In summary, to compute the average controllability value for node i in  $\mathbf{A}$ , we compute the  $\operatorname{Trace}(\mathbf{W}_{\mathscr{H}})$  when node i is the only control node (i.e.  $\mathbf{B}_{\mathscr{H}} = e_i$ ).

Modal controllability refers to the ability of a node to control the evolutionary modes of a dynamical network, and is most interpretable when used to identify states that are poorly controllable given  $\mathbf{B}_{\mathscr{K}}$ . To calculate modal controllability, one must first obtain the eigenvector matrix  $V = [v_{ij}]$  of the adjacency matrix  $\mathbf{A}$ . If  $v_{ij}$  is small, then the j-th evolutionary mode of the input-independent form of Eq. (1),  $\mathbf{x}(t) = \mathbf{A}\mathbf{x}(t)$ , is poorly controllable from node i. Following prior work (Pasqualetti et al., 2014), we define  $\phi_i = \sum_{j=1}^N (1 - \xi_j^2(\mathbf{A}))v_{ij}^2$  as a scaled measure of the modal controllability of each of the N modes  $\xi_0(\mathbf{A}), \ldots, \xi_{N-1}(\mathbf{A})$  from node i.

Finally, we calculate the mean of the regional controllability values either across the whole brain (Fig. S1) or within the cortex and subcortex separately (Figs. 3–6). For each subject, we define the mean modal

controllability to be the sum of the values of  $\phi_i$  for each node within **A**, divided by the number of regions. Similarly, we define the mean average controllability to be the sum of the values of  $\text{Trace}(\mathbf{W}_{\mathscr{X}})$  for each node within **A**, divided by the number of regions.

## 2.8. Linear regressions involving network control metrics and cognitive performance

For all analyses of network control metrics, we examined the effect of sex while controlling for age, total brain volume (segmented brain volume, as defined by FreeSurfer BrainSegVol metric), handedness, and motion during the diffusion scan. We used multiple ordinary least squares (OLS) linear regression with the lm() command in R (R Core Team, 2017) to fit the following general equation:

$$C = 1 + \beta_a a + \beta_v v + \beta_h h + \beta_{md} m_d + \beta_s s , \qquad (4)$$

where C is the controllability statistic (either  $\phi_i$  for modal controllability or  $\mathcal{A}$  for average controllability), a is age, v is total intracranial volume,  $m_d$  is the mean framewise displacement as a summary measure of inscanner head motion during the diffusion imaging sequence, h is handedness, and s is sex. We then used the R package visreg (Breheny and Burchett, 2013) to calculate 95% confidence intervals around fitted lines and generate partial residuals. Multicollinearity between predictors in regression models can confound estimates of individual predictor weights. Therefore, we computed the variance inflation factors (VIFs) (Obrien, 2007; Fox et al., 2012) for age, brain volume, handedness, head motion, and sex as a predictor set. This analysis demonstrated VIFs ranging from near 1 (the minimum possible VIF) to 1.5, well below the conservative threshold of 5 (Obrien, 2007), suggesting that collinearity between predictors was low (Fig. S7b).

We also used linear regression to test whether regional network control metrics explain variance in CPT false positives while controlling for age, total brain volume, handedness, head motion, and sex. We carried this out by fitting the following equation:

$$F = 1 + \beta_C C + \beta_a a + \beta_v v + \beta_h h + \beta_{md} m_d + \beta_s s , \qquad (5)$$

where F is the false positive rate on the CPT and all other variables are the same as above. For node-level analyses of controllability, we applied a false discovery rate (FDR) correction (Benjamini and Hochberg, 1995) (q < 0.05) over all nodes to control for Type I error due to multiple testing.

#### 2.9. Non-linear fits of network metrics

Following Ref. (Tang et al., 2017), we used non-linear models to examine the relationships between synchronizability, average controllability, and modal controllability (Fig. 5). Synchronizability measures the tendency of a network to maintain a stable, global activity state (Tang et al., 2017; Pecora and Carroll, 1998), in contrast to network controllability, which quantifies the capacity for each node to drive transitions to new states (Gu et al., 2015). By assaying the contrasting metric of synchronizability, we provide support for the specificity of sex differences to control dynamics. We generated estimates of parameters for models of the form  $y = a + b \exp(cx)$  via non-linear least squares using the nls() function in R. To compare these fits between males and females, we performed an analysis of variance (ANOVA). For example, when considering sex differences in the nonlinear relation between modal controllability and average controllability, we examined the expression:

$$\phi_i = (a + \alpha s) + (b + \beta s) \exp((c + \gamma s) \mathcal{A}), \tag{6}$$

where  $\phi_i$  is modal controllability,  $\mathscr A$  is average controllability, and s is sex, coded as 0 for males and 1 for females, so that  $\alpha$ ,  $\beta$ , and  $\gamma$  each equal zero for males and the equation is reduced to the base form. The predicted values for males or females obtained from the full model were

used to generate the curves shown in Fig. 5.

#### 2.10. Linear regression of bold data on network control metrics

Finally, and in keeping with our linear systems framework, we sought to test whether controllability would predict brain state  $(\mathbf{x}(t))$  as defined by BOLD activation during a working memory task. In these analyses (Fig. 8), we used the residuals from Eq. (4) for controllability. For activation, we used the residuals from the following equation:

$$M = 1 + \beta_a a + \beta_b h + \beta_{mn} m_n + \beta_s s, \tag{7}$$

where M is 2-back minus 0-back activation (hereafter referred to as "activation"), a is age, h is handedness,  $m_n$  is the mean framewise displacement during the n-back working memory scan, and s is sex. Because we had no prior knowledge about where controllability might predict activation, we fit linear models between controllability and activation at every possible pair of nodes; that is, we performed  $234 \times 234$  regressions of controllability residuals at each node with activation residuals at each node. The  $234 \times 234$  matrices of p-values for the slope of controllability on activation were FDR corrected (q < 0.05) separately for average controllability and for modal controllability. To identify regions where activation was associated with executive function, we followed previous work (Satterthwaite et al., 2013; Shanmugan et al., 2016) by examining d, a composite measure of n-back task performance which takes both correct responses and false positives into account to separate performance from response bias.

When testing for an interaction between controllability and sex as a predictor of n-back activation, we defined  $C_r$  as the residuals from the following equation:

$$C = 1 + \beta_a a + \beta_v v + \beta_h h + \beta_{md} m_d, \tag{8}$$

and we defined  $M_r$  as the residuals from the following equation:

$$M = 1 + \beta_a a + \beta_v v + \beta_h h + \beta_{mn} m_n, \tag{9}$$

where all variable names are the same as above. We carried out this procedure so as to remove biases of other covariates from controllability and activation values while not removing the effects of sex, in order to fit the following model:

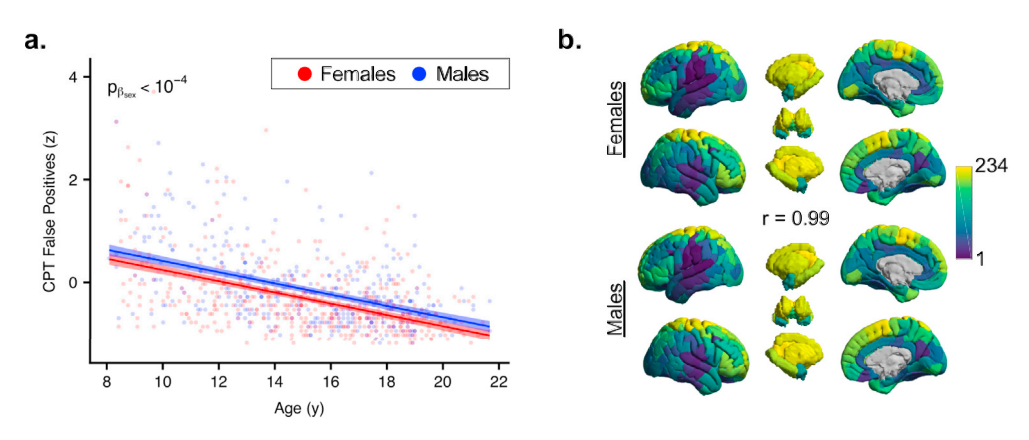
$$M_r = 1 + \beta_{C_r} C_r + \beta_s s + \beta_{C_{S_{int}}} s C_r$$
, (10)

again for every possible pair of  $234 \times 234$  nodes for average and modal controllability, where  $\beta_{Cs_{int}}$  represents the coefficient for the interaction term between controllability residuals and sex. We applied FDR correction (q < 0.05) separately for average and modal controllability.

#### 3. Results

#### 3.1. Sex differences in executive function

Our analysis of sex differences in the development of executive function and its neurobiological underpinnings began with a sex-stratified comparison of performance on the continuous performance task (CPT) (Gur et al., 2010), a task designed to measure sustained attention and impulsivity. In our sample, there was no sex difference in CPT true positive rate, which reflects sustained attention. Thus, we focused on the false positive rate in order to capture impulsivity. Sex differences in CPT impulsivity have been replicated in large studies (Hasson and Fine, 2012; Riley et al., 2016), may underlie increased risk taking in males (Cross et al., 2011), and map intuitively to the notion of brain network control. CPT false positives were significantly higher in males (full model  $r^2=0.25$ , df=866,  $p=3.8\times10^{-5}$ , Cohen's  $f_{sex}^2=0.02$ , Cohen's  $f_{age}^2=0.31$ ; Fig. 2a) with no interaction between age and



2. Cognitive development network controllability by sex. (a) False positive rate on the continuous performance task (Gur et al., 2010), a measure of impulsivity and inhibition, displayed a linear relationship to age. Red and blue data points and curves represent females and males, respectively. Each point represents a subject's partial residual with respect to sex; solid lines represent the predicted mean for males and females separately, and shaded envelopes denote 95% confidence intervals of the prediction. (b) Rank of mean average controllability values at each node across 389 male subjects and 490 female subjects, separately. The Spearman rank correlation between regional average controllability averaged across males and regional average controllability averaged across females was r =0.9915.

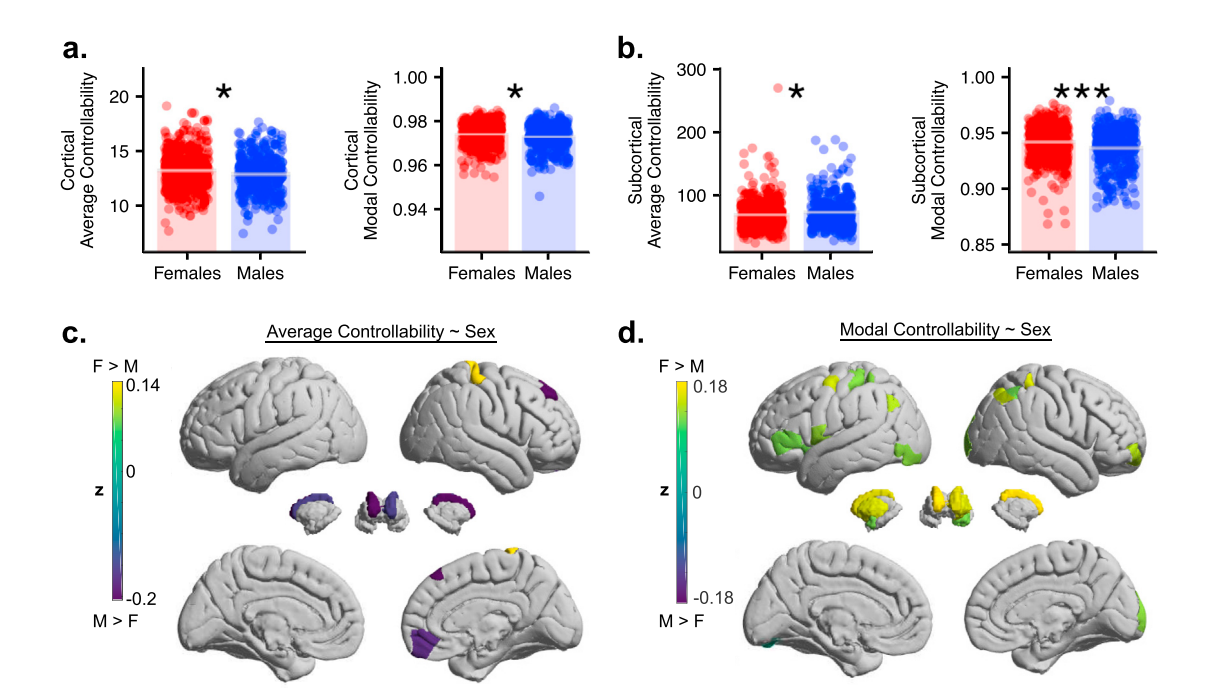


Fig. 3. Sex differences in regional controllability. (a-b) Controllability estimates averaged over 219 cortical nodes (a) and 14 subcortical nodes (b), for average controllability and modal controllability. Females have higher cortical average controllability, cortical modal controllability, and subcortical modal controllability, but males have higher subcortical average controllability. In panels a-b, red and blue represent females and males, respectively. Each point represents a subject's partial residual with respect to sex; bar height represents the predicted mean for males and females separately, and shaded grey envelopes denote 95% confidence intervals of the prediction. (c-d) Heatmaps where color intensity corresponds to standardized regression coefficients for sex, with warmer colors indicating higher controllability in females. Average controllability is depicted in panel (c) and modal controllability is depicted in panel (d). Colors reflect values of standardized regression coefficients for controllability at each node as a predictor of executive function while controlling for covariates (Eq. (4)). \*, p < 0.05, \*\*, p < 0.01, \*\*\*, p < 1 × 10<sup>-4</sup>.

sex. Furthermore, CPT false positives decreased with age ( $p < 10^{-15}$ ; Fig. 2a). This result suggests that the development of impulse control occurs via a similar course for males and females, but that males exhibit higher impulsivity in this particular task for all ages studied. After performing this sex-stratified analysis of the developmental course of impulsivity, we next turned to a consideration of its potential neurobiological underpinnings (Fig. 1a).

#### 3.2. Sex differences in regional network controllability

Our general hypothesis was that sex differences in executive function in youth stem from sex differences in the controllability of structural brain networks as they rewire over development. Notably, this notion bridges the control of behavior (executive function, impulse control)

with the control of brain dynamics (network controllability). To test this hypothesis, we examined the anatomical distribution of control points in the structural brain networks of males and females separately. We ranked the mean average controllability value at each region for males and females separately, which revealed that the distribution of controller strength is virtually identical between males and females (r=0.99; Fig. 2b). This result suggests that there is no sex difference in the spatial distribution of controllers when classified by their relative magnitudes. This finding is consistent with meta-analyses suggesting that if sex differences in neurological and cognitive phenotypes exist, they are limited to a few specific cognitive domains (Hyde, 2014; Joel, 2012).

We next investigated whether the actual (rather than ranked) regional controllability estimates differed by sex. We addressed this question first by considering the cortex and subcortex separately, moti-

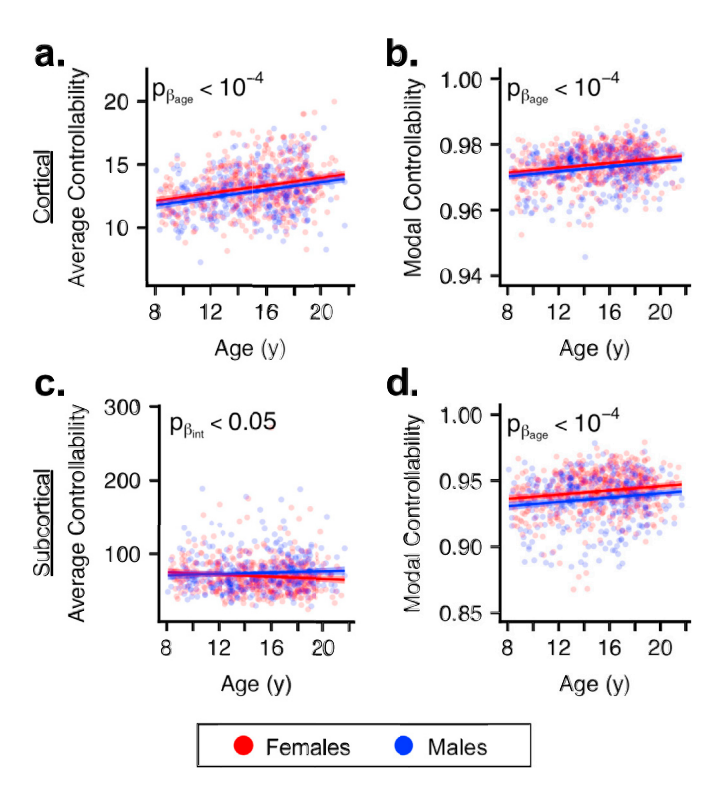


Fig. 4. Network controllability as a function of age. (a-d) Relationship between age and controllability estimates, averaged over 219 cortical nodes (a-b) and 14 subcortical nodes (c-d), for average controllability (a, c) and modal controllability (b, d). Modal controllability increases with age in the cortex and in the subcortex; average controllability increases with age in the cortex. In the subcortex, the p-value for the age-by-sex interaction for average controllability was < 0.05, although it was not significant after correcting for the false discovery rate (q < 0.05). Moreover, the simple slopes for males  $(\beta_{age})$  and females  $(\beta_{age} + \beta_{age \times sex})$  were not significantly different from 0. Age-by-sex interactions in panels a, b, and d were not significant. Red and blue represent females and males, respectively. Each point represents a subject's partial residual with respect to age; lines represent regression slopes for males and females separately, and shaded envelopes denote 95% confidence intervals of the slopes. The p values for  $\beta_{age}$  are shown in panels (a, b, d) and for  $\beta_{age \times sex}$  are shown in panels (a, b, d) and for  $\beta_{age}$  are shown in panels (a, b, d) and for  $\beta_{age}$  are shown in panels (a, b, d) and for  $\beta_{age}$  are shown in panels (a, b, d) and for  $\beta_{age}$  are shown in panels (a, b, d) and for  $\beta_{age}$  are shown in panels (a, b, d) and for  $\beta_{age}$  are shown in panels (a, b, d) and for  $\beta_{age}$  are shown in panels (a, b, d) and for  $\beta_{age}$  are shown in panels (a, b, d) and for  $\beta_{age}$  are shown in panels (a, b, d) and for  $\beta_{age}$  are shown in panels (a, b, d) and for  $\beta_{age}$  are shown in panels (a, b, d) and for  $\beta_{age}$  are shown in panels (a, b, d) and for  $\beta_{age}$  are shown in panels (a, b, d) and for  $\beta_{age}$  are shown in  $\beta_{age}$  are shown in

vated by the notion of top-down (i.e. cortical) versus bottom-up (i.e. subcortical) control of behavior (Heatherton and Wagner, 2011) relevant to impulse control (Brewer and Potenza, 2008). Specifically, we computed mean controllability values for each subject across 219 cortical regions and 14 subcortical regions. In the cortex, mean average controllability ( $r^2 = 0.083$ , df = 873, p = 0.018, Cohen's  $f_{sex}^2 = 0.0065$ ; Fig. 3a) and mean modal controllability ( $r^2 = 0.13$ , df = 873, p = 0.016, Cohen's  $f_{sex}^2 = 0.0067$ ; Fig. 3a) are higher in females. Mean modal controllability in the subcortex is also higher in females ( $r^2 = 0.046$ ,  $df = 873, p = 7.5 \times 10^{-5}$ , Cohen's  $f_{sex}^2 = 0.018$ ; Fig. 3b), whereas mean average controllability in the subcortex is higher in males ( $r^2 = 0.036$ , df = 873, p = 0.041, Cohen's  $f_{sex}^2 = 0.0048$ ; Fig. 3b). All analyses of sex differences in cortical and subcortical average and modal controllabillity were statistically significant after controlling the false discovery rate (q < 0.05). Only in the subcortex did males have higher average controllability than females; this result suggests that the connectivity profile of subcortical regions may contribute to sex differences in functional brain dynamics.

In a finer-grained analysis, we investigated whether the controllability of single regions differed by sex. Modal and average controllability were separately examined at each region, while accounting for age, total brain volume, handedness, and mean in-scanner head motion as model covariates. We found that average and modal controllability differed by

sex at a subset of network nodes after FDR correction (q < 0.05) for multiple comparisons. Nodes with average controllability values that differed by sex were almost all (4/5) higher in males and located in the frontal lobe or subcortex (Fig. 3c-d). Conversely, nodes with modal controllability values that differed by sex were all (18/18) higher in females and located in frontoparietal and subcortical systems. Cohen's  $f^2$ effect sizes for sex as a predictor of regional controllability ranged from 0.0097 - 0.030, indicating small effects. Average and modal controllability may be highly negatively correlated depending on the network topology (Wu-Yan et al., 2018), but we show that the covariance between average and modal controllability depends on both the subject and the brain region (Figs. S2a-c), supporting distinct interpretations of each metric. We also analyzed sex differences in boundary controllability, which quantifies the extent to which a region is poised to coordinate activity between modules (Gu et al., 2015). However, we only found a sex difference at one region (see Supplemental Text for discussion of findings; Fig. S8b) and thus we focus the remainder of our analysis on average and modal controllability. These results suggest that controller strength differs between males and females in a regionally specific and control strategy specific manner.

#### 3.3. Development of network controllability across the sexes

We next turned to an assessment of whether developmental trends of network controllability differed by sex. We found that controllability in the cortex and subcortex tended to increase with age, with the exception of average controllability in the subcortex. In the cortex ( $r^2 = 0.13$ , df =873,  $p=5.5 imes 10^{-10}$ , Cohen's  $f_{age}^2=0.045$ ; Fig. 4b) and subcortex ( $r^2=1.00$ ) 0.046, df = 873,  $p = 1.2 \times 10^{-5}$ , Cohen's  $f_{age}^2 = 0.022$ ; Fig. 4d), mean modal controllability increases with age for males and females. Mean cortical average controllability also increases with age ( $r^2 = 0.083$ , df =873,  $p=1.7\times 10^{-15}$ , Cohen's  $f_{age}^2=0.075$ ; Fig. 4b). Interestingly, there was a weak age-by-sex interaction only with subcortical average controllability that did not survive FDR correction (q < 0.05), such that the slope was positive for males and negative for females ( $r^2 = 0.041$ , df = 872, p = 0.024, Cohen's  $f_{int}^2 = 0.0059$ ; Fig. 4c). However, we found that subcortical average controllability remains stable throughout development for both males ( $eta_{age}=0.51, t=1.30, p=0.19, df=872$ ) and females  $((\beta_{ace} + \beta_{ace*sex}) = -0.68, p = 0.06, t = -1.89, df = 872)$ (Preacher et al., 2004). Taken together, these results suggest that controllability changes with age similarly for males and females, but that average controllability in the subcortex is static during development, unlike modal controllability or cortical average controllability.

With the knowledge that controllability has a sex-independent relationship with age, we were interested in testing the hypothesis that sex influences the relationship between different types of controllability in the developing brain. Following prior work characterizing the developmental course of network control properties (Tang et al., 2017), we fit the relationships between average and modal controllability with the exponential function  $y = a + b \exp(cx)$  separately for each sex (Eq. (6)). Our results showed that males and females did not have a statistically different relationship between average and modal controllability averaged across the whole brain (p = 0.14, df = 3; Fig. 5a,e). In the cortex alone, average and modal controllability followed an increasing exponential form (Fig. 5b,f), similar to that of the whole brain. In contrast, in the subcortex alone average and modal controllability followed a decreasing exponential form (Fig. 5d,h). When sex was included in the model, fits improved significantly (cortex:  $p = 1.8 \times 10^{-8}$ , df = 3, Fig. 5b,f; subcortex:  $p = 7.0 \times 10^{-9}$ , df = 3, Fig. 5c,g), suggesting that these regions may contain sex-dependent differences in structural connections important for controlling brain network state transitions via different strategies.

Next, we performed a specificity analysis to determine whether our results could be further confirmed by sex differences in a contrasting

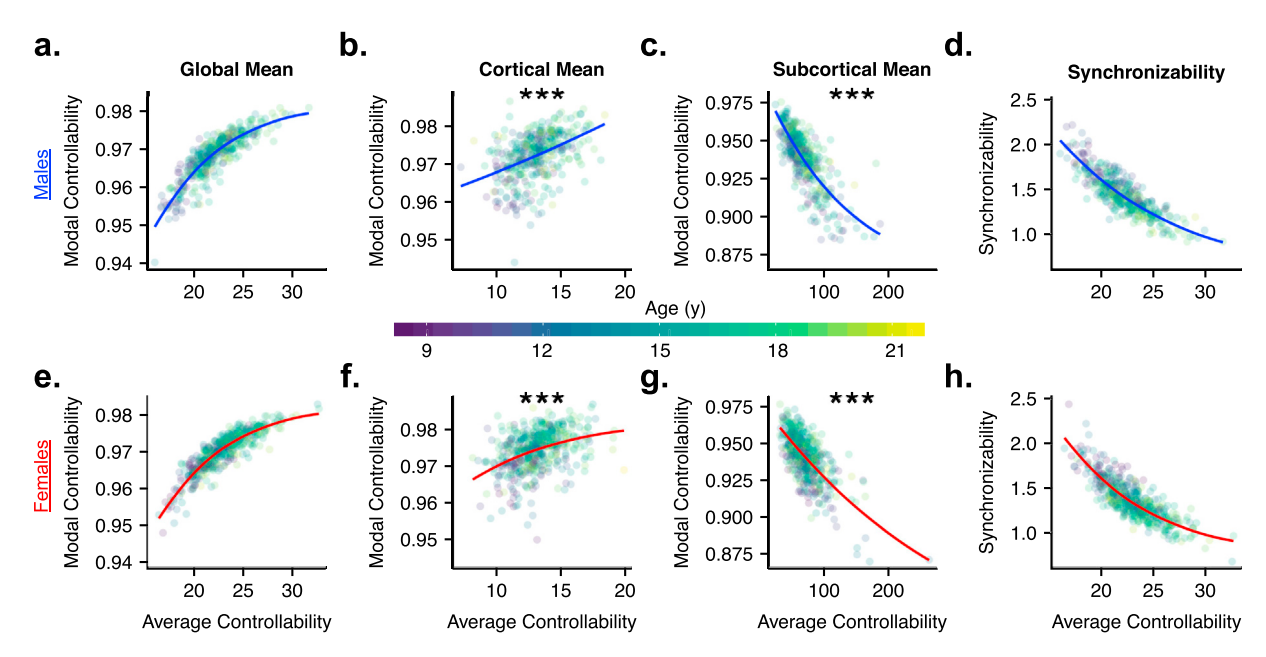


Fig. 5. Sex effects on relationships between metrics of network control and dynamics. Relationships between whole-brain average and modal controllability (a, e), between synchronizability and whole-brain average controllability (d, h), and between regional average controllability and regional modal controllability (b-c, f-g). Data from male subjects is depicted in panels (a-d) and data from female subjects is depicted in panels (e-h). Non-linear least squares was used on the base model:  $y = a + b^* \exp(c^*x)$ , and the full model:  $y = (a + \alpha^* \operatorname{Sex})\operatorname{Sex})\operatorname{Sex})x$ ). Slopes represent coefficients from the full model. The p values were obtained from an ANOVA comparing base and full models. In these cases, a low p-value indicates that allowing for a sex term in the model significantly increases the explained variance. \*, p < 0.05, \*\*, p < 0.01, \*\*\*,  $p < 1 \times 10^{-4}$ .

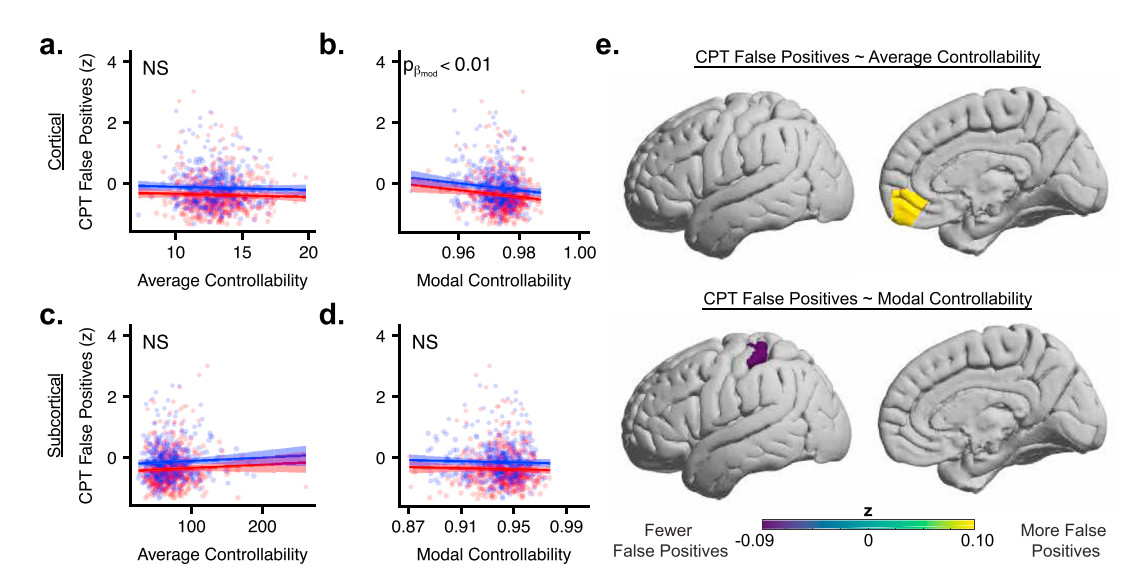


Fig. 6. Network controllability and cognitive performance. (a-d) Relationship between age and controllability estimates, averaged over 219 cortical nodes (a-b) and 14 subcortical nodes (c-d), for average controllability (a, c) and modal controllability (b, d). Cortical modal controllability (b) is positively correlated with CPT false positive rate while cortical average controllability (a) is not significantly correlated with CPT false positive rate. Subcortical controllability (c-d) is not significantly related to CPT false positive rate. In panels (a-d), red and blue represent females and males, respectively. Each data point represents a subject's partial residual with respect to controllability; lines represent regression slopes for males and females separately, and shaded envelopes denote 95% confidence intervals of the slopes. (e) Brain regions with sex-associated average (top) or modal (bottom) controllability and their relation to CPT false positive rate (FDR corrected, q < 0.05). Colors reflect values of standardized regression coefficients for controllability at each node as a predictor of CPT false positive rate while controlling for covariates. For panels (a-e), there were no significant sex-by-controllability interactions on CPT false positive rate.

metric – synchronizability – that probed the susceptibility of the network to be constrained within a narrow (rather than broad) range of dynamics. We found that synchronizability did not differ between males and females (S1b) and decreased with age in a sex-independent fashion (S1d). Moreover, the exponential relationship between synchronizability and average controllability did not differ by sex (p=0.33, df=3; Fig. 5d,h), confirming the local (Fig. 3c–d) rather than global (Fig. 2b) differences in

metrics of network control and dynamics.

3.4. Sex differences in network controllability predict individual differences in executive function

While sex differences in network controllability are of interest in understanding the structural drivers of brain dynamics, their impact on

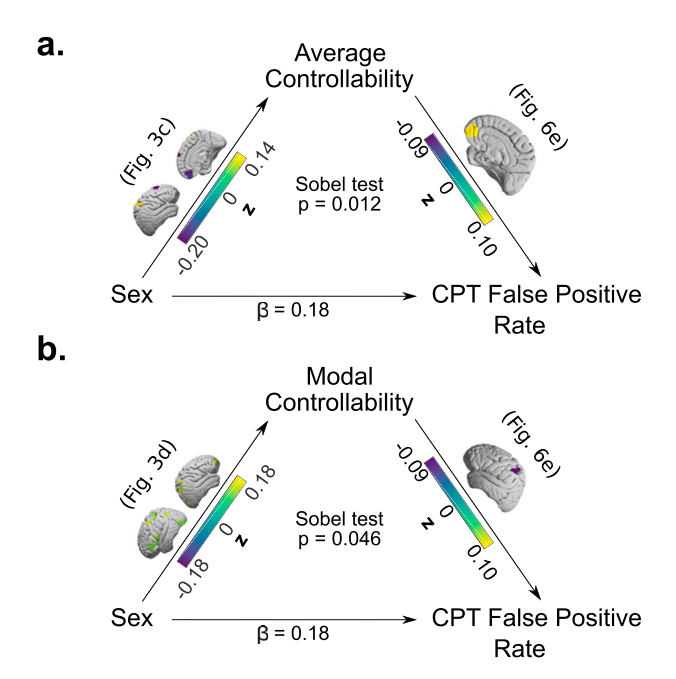


Fig. 7. Controllability mediates the relationship between sex and executive function.  $(a \cdot b)$  Sobel mediation testing (Sobel, 1982; Baron and Kenny, 1986; Wang, 2018) for sex  $\rightarrow$  controllability  $\rightarrow$  CPT false positive rate, using control nodes that are associated with sex and predict CPT false positive rate. The only regions displaying these relationships are the right medial orbitofrontal lobe (average controllability; panel (a)) and the left postcenteral gyrus (modal controllability; panel (b)). Associations between sex and controllability from Fig. 3c and d are shown; cooler colors indicate higher controllability in males. Age, total brain volume, handedness, and head motion were regressed out of controllability values and age was regressed out of CPT false positives prior to Sobel testing.

behavior requires a link to cognition. Here we examine the relation between impulsivity on the CPT and network controllability across cortex and subcortex separately, and then at individual brain regions, while controlling for age, brain volume, handedness, head motion, and sex. When considering mean subcortical controllability and CPT false positives we found that neither average ( $r^2=0.25$ , df=862, p=0.23, Cohen's  $f_{ave}^2=0.0017$ ; Fig. 6c) nor modal ( $r^2=0.25$ , df=862, p=0.48, Cohen's  $f_{mod}^2=5.8\times10^{-4}$ ; Fig. 6d) controllability in the subcortex was associated with impulsivity. A different trend was apparent in the cortex: average controllability was not significantly related to false positives ( $r^2=0.25$ , df=862, p=0.37, Cohen's  $f_{mod}^2=9.3\times10^{-4}$ ; Fig. 6a), while modal controllability was significantly negatively related to false positives after FDR correction ( $r^2=0.25$ , df=862,  $p=4.3\times10^{-3}$ , Cohen's  $f_{mod}^2=0.0095$ ; Fig. 6b).

Next, we considered the 21 brain areas that we had previously found to display sex differences in controllability values (5 nodes for average controllability and 18 nodes for modal controllability, with 2 nodes overlapping). Among nodes with sex differences in average controllability, average controllability at the right medial orbitofrontal cortex was higher in males and positively related to impulsivity (Cohen's  $f_{ave}^2 = 0.014$ , FDR corrected, q < 0.05; Fig. 6e). Among nodes with sex differences in modal controllability, modal controllability at the left post-central gyrus was higher in females and negatively related to impulsivity (Cohen's  $f_{mod}^2 = 0.011$ , FDR corrected, q < 0.05; Fig. 6e).

One parsimonious explanation for these results is that controllability mediates the relationship between sex and impulsivity. We explicitly tested for such a mediation and found that, indeed, average controllability at the right medial orbitofrontal cortex (Fig. 7a) and modal controllability at the left postcentral gyrus (Fig. 7b) were statistically significant mediators of the relationship between sex and CPT false

positives. Taken together, these results suggest that increased orbito-frontal average controllability and decreased postcentral modal controllability may be biomarkers of impulsivity in males. Interestingly, however, we found that controllability at several regions without sex-associated controllability values was associated with impulsivity (Figs. S9a-b), suggesting that structural network controllability may explain individual differences in impulsivity outside of the context of sex differences. We also tested for interactions between sex and regional controllability values as predictors of CPT false positives, which would indicate a sex-dependent relationship between regional controllability and impulsivity. We found statistically significant interactions between sex and average controllability at somatomotor regions, but the simple slopes for males and females did not differ from 0 (see Supplemental Text for discussion of results; Fig. S9c).

### 3.5. Relationship between sex, n-back task activation magnitudes, and controllability

Describing the relationship between sex, regional controllability, and impulsivity provides us with a better understanding of the importance of structural brain networks in sex differences in executive function. The final aspect of our hypothesis pertains to whether network control theory can be used to explain how differences in brain network structure produce divergent patterns of brain activity that underpin other domains of executive function, such as working memory. We hypothesized that regional controllability values would predict regional n-back task activation magnitudes, and that associations between controllability and activation would differ by sex.

To obtain a reference point for activation profiles associated with strong executive function, we separately regressed activation at each node on d (Satterthwaite et al., 2013). This analysis identified 113 nodes for which activation was associated with successful task performance (Fig. 8a, left). Note that in contrast to the use of CPT false positive rate in the previous analyses, here we considered the d measure to summarize performance on the n-back task only (Snodgrass and Corwin, 1988) so that the performance measure is directly related to the context in which activation values are measured. Consistent with prior results (Satterthwaite et al., 2013), we found that relative deactivation of default mode network regions (Raichle, 2015) (i.e. posterior cingulate and medial prefrontal cortex) as working memory load increased was predictive of performance. Interestingly, males exhibited reduced deactivation in the posterior cingulate cortex with increasing working memory load (FDR corrected, q < 0.05; Fig. 8a, right).

After identifying regions at which activation was associated with executive function, we sought to relate these activation values to controllability metrics of structural brain networks. We found that increasing average controllability was only positively related to activation (Fig. 8b). Average controllability at the right transverse temporal gyrus was associated with activation at 7 different regions, which cluster together in a symmetric fashion in inferior temporal cortex (Fig. 8c). Modal controllability was not significantly associated with activation.

Next, we tested our hypothesis that the relationship between regional controllability and activation depends on sex. Specifically, we performed the same analysis on males and females, separately. Consistent with the pooled analysis, the profile of controllability-activation associations overlapped significantly between the sexes (Fig. 8d, Fig. S5a). While there was no overlap in the precise regions involved in these sex-split analyses, there were gross anatomical similarities between males and females. In both sexes, controllability at temporal regions was associated with activation at lateral frontal regions. We observed significant interactions between controllability and sex in predicting activation (Fig. S5c), such that controllability at middle and inferior temporal lobe were more positively related to activation in females (Fig. S5a) than in males (Fig. S5b). These results support the notion that both similarities and differences in structure-function relationships exist across the sexes.

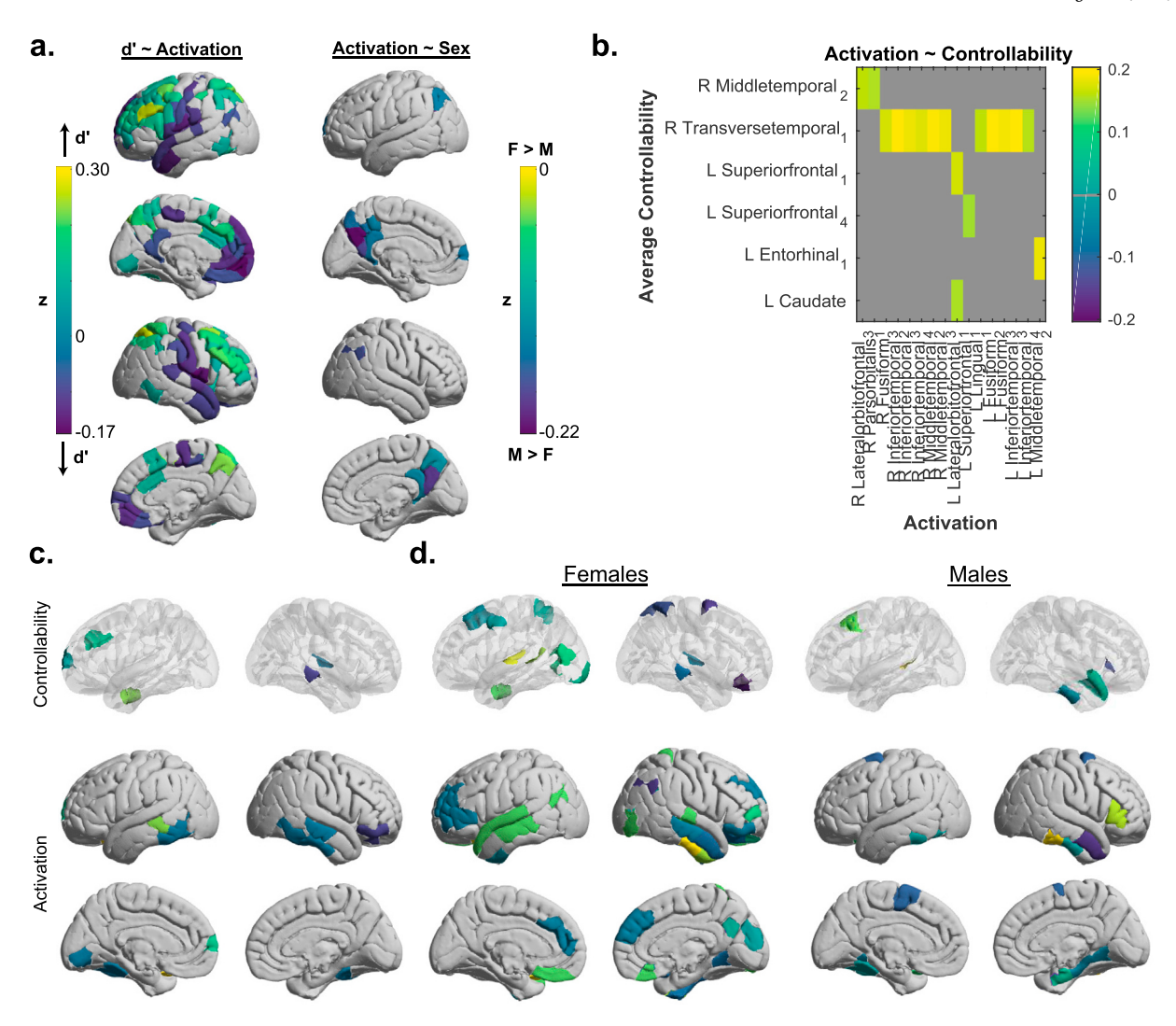


Fig. 8. Regional controllability predicts n-back task activation and cognitive performance differently for males and females. (a) Brain regions at which the 2-back minus 0-back GLM  $\beta$  weights are associated with 2-back d, a summary measure of task performance (left), or sex (right), in n = 837 subjects with quality fMRI data. (b) Heatmap depicting standardized multiple linear regression  $\beta$ 's for regional average controllability as a predictor of regional 2-back minus 0-back activation. Only nodes with associations surviving FDR correction are shown (q < 0.05). (c) Visual representation of the data presented in panel (b); average controllability at highlighted nodes is associated with activation at nodes of the same colors. (d) Associations between activation and average controllability for n = 365 males and n = 472 females, separately. Modal controllability was not significantly associated with activation. For panels (c,d), corresponding colors indicate association between control node and regional activation.

#### 4. Discussion

Our study demonstrates that network control theory can be used to explain how differences in brain network structure produce divergent patterns of brain activity that underpin executive function and its domain-specific differences across males and females. We first showed that the relative locations of controllers by strength did not differ between males and females, suggesting that the overall structure of control points is similar across the sexes. Then, we showed that controllability covaried with age in a sex-independent fashion in both the cortex and subcortex. While global and developmental sex differences appear minimal, local sex differences in controllability exist and predict false positives on a CPT, a common measure of impulsivity. Notably, average and modal controllability significantly mediated the associations between sex and CPT false positive rate, such that male controllability profiles are negatively associated with impulsivity on the CPT. Crucially, consistent with predictions from network control theory, we also observed associations between nodal average controllability and n-back task BOLD activation magnitudes that differ by sex, suggesting that network control theory can help predict how differences in brain network structure may

manifest in different activity patterns.

#### 4.1. Implications for cognitive and clinical neuroscience

Impulsivity is generally higher in males (Hasson and Fine, 2012; Gur et al., 2012; Riley et al., 2016; Chapple and Johnson, 2007), which is reflected in higher rates of criminality (Cross et al., 2011) and substance use (Romer et al., 2009; Weafer and de Wit, 2014). While it is known that sex differences exist in the prevalence of disorders of executive function (Cross et al., 2011) and the putative neural circuitry involved (Castellanos and Tannock, 2002; Pohjalainen et al., 1998), it is unclear whether the pathophysiology of such disorders is sex-specific or sex-independent. Our study significantly extends the boundaries of knowledge in demonstrating neurophysiological markers of sex differences in CPT false positive rate, and in couching such markers within a general network control theory of brain function.

The present work also provides important groundwork for clinical therapy. The delivery of psychiatric care is shifting towards personalized, targeted interventions. This shift can be supported by the methodology and computational tools of network neuroscience, where accurate

models of brain structure and dynamics can be constructed for single individuals (Stephan et al., 2017; Izhikevich and Edelman, 2008). Such subject-, age-, and sex-specific models of brain structure and function can directly inform neuromodulatory therapies such as transcranial magnetic stimulation by offering predictions about how stimulation will affect both the area being stimulated, and other areas connected to it, thereby producing a complex spatiotemporal influence on brain state. Specifically, assuming a model of brain dynamics allows us to determine which nodes could most easily drive transitions in the state of brain activity via some stimulatory input. The network control theory that we use here to study the internal modulation of brain state (via undertaking a task requiring executive function) also makes explicit predictions about the external modulation of brain state (via stimulation or neurofeedback) (Murphy and Bassett, 2017). Indeed, average controllability values were associated with sex-dependent, symmetric patterns of brain activity (Fig. 8c-d). Our results suggest that average controllability values explains variance in brain state, beyond what can be predicted from a simple streamline-weighted adjacency matrix. Notably, however, estimated effect sizes of sex on controllability, and of controllability on performance, were in ranges considered small, and thus the practical importance of the observed sex differences are still unclear. Nevertheless, these observations are the first steps towards a characterization of brain dynamics that would allow clinicians to predict the impact of stimulation given a subject-, age-, and sex-specific network architecture, thereby producing predictable changes in brain state.

An understanding of the relation between network controllability, sex, and executive function could provide important context for the study and diagnosis of neurological disease and psychiatric disorders whose prevalence may differ by sex and whose presentation includes alterations in executive function. In our study, the most robust associations between controllability, sex, and impulsivity were found in the right ventromedial prefrontal cortex and the left superior parietal lobe.

It is widely known that the prefrontal cortex is important for behavioral planning and working memory (Tanji and Hoshi, 2008; Euston et al., 2012; Eriksson et al., 2015), two key components of executive function. Decreased volume in the right ventromedial prefrontal cortex (vmPFC) specifically has been previously implicated in impulsive behaviors among adolescent males (Boes et al., 2008). Injury to vmPFC has been associated with reduced motor impulse control, aggression, and violence (Brower and Price, 2001; Bechara and Van Der Linden, 2005). Activity in right vmPFC has been shown to increase in adults during response inhibition (Horn et al., 2003), yet is reduced in individuals with alcohol dependence (Li et al., 2009). Moreover, regional activation in medial prefrontal cortex has been shown to differ between males and females (Straube et al., 2009; Goldstein et al., 2005). Clearly, both structure and function of right medial prefrontal cortex play an important role in impulse control and may differ by sex. Our demonstration that the local control properties of right vmPFC differ by sex and explain impulsive behaviors helps link these prior findings to a dynamical systems framework. Specifically, individuals with high average controllability in vmPFC may exhibit local structural topology that facilitates transitions away from brain states underlying impulsive behavior.

Activity in the superior parietal cortex is also critical for working memory (Eriksson et al., 2015), especially in rearranging or manipulating information (Koenigs et al., 2009). While superior parietal cortex is not typically tied to impulse control, gray matter volume in the parietal lobe has been found to peak earlier in females than in males (Lenroot et al., 2007; Giedd et al., 1999). In light of these previous findings, our study provides an important account of sex differences in white matter connectivity profiles at medial frontal and superior parietal cortex from the dynamical perspective of network control theory. For instance, the relationship between average controllability and working memory task activation might suggest that this task involves transitions to nearby states. Additionally, the finding that impulsivity was more strongly related to somatomotor average controllability in males suggests that

increasing average controllability can also support transitions that are unfavorable for certain behaviors. Superior parietal modal controllability was higher in females and negatively associated with impulsivity, which may indicate that these regions exhibit greater support in females for transitions to distant states important for impulse control. Overall, our results suggest that the connectivity profile of frontoparietal structures is related to sex and is important for executive function, supporting the notion that altered structural connectivity is a key feature of disorders of executive function.

#### 4.2. Methodological considerations

Several methodological considerations are pertinent to this work. First, we use a time-invariant, linear model of brain dynamics because its network control properties have been well characterized mathematically. However, it is known that the brain is highly non-linear and explained well by models incorporating noise (Izhikevich and Edelman, 2008; Deco et al., 2011). Yet, the associations between controllability and brain activity that we uncover here suggest that a simple linear model is sufficient to capture some aspect of the underlying brain dynamics. Our observations beg the question of how and when linear approximations of nonlinear dynamics can be useful. As is relatively intuitive, linear approximations of nonlinear dynamics hold true over short time horizons and in the vicinity of the system's current operating point (Leith and Leithead, 2000). Additional evidence suggests that time averaged dynamics and slow fluctuations in the blood-oxygen-level-dependent signal can also be reasonably modeled with assumptions of linearity (Honey et al., 2009; Galan et al., 2008; Gu et al., 2018). Moreover, even when the dynamics of a system are truly nonlinear, one can ask whether the predictions of control from the linear model can be used to infer the response of the nonlinear system, either statistically or formally (Coron, 2009; Whalen et al., 2015). Initial evidence in neural systems suggests that controllability statistics derived from the linear model of network dynamics can be used to predict transitions into and out of bursting regimes in neuronal ensembles (Wiles et al., 2017) and changes in activity states induced by stimulation in Wilson-Cowan oscillator models of cortical columns (Muldoon et al., 2016). Nevertheless, it remains an important and interesting direction to build on the emerging approaches for nonlinear control in the physics and engineering literature (Motter, 2015) to better understand the control of nonlinear brain dynamics.

Second, axons transmit information in a unidirectional fashion, but diffusion imaging and associated tractography tools cannot elucidate the directionality of large axonal fiber bundles. Thus, we construct a symmetric adjacency matrix A, assuming bidirectional influence between network nodes, and all interpretations of regional controllability depend on the realism of that assumption. The assumption is supported by evidence from tract tracing in macaques that the majority of connections at this large scale are bidirectional (Bassett and Bullmore, 2017), and by computational studies demonstrating that controllability statistics are largely conserved across directed and undirected mesoscale connectomes (Kim et al., 2018). Yet, it is nevertheless important to acknowledge that the eigenvalues of a symmetric matrix can only ever be real and thus the system will not oscillate, as neural systems are known to do. It will be interesting in future to consider approaches to study the control of oscillatory activity in the brain, and to validate those approaches with high-resolution data such as electrocorticography.

Additionally, streamline counts and network density vary between scans (Zhu et al., 2011) and with different tract reconstruction methods (Maier-Hein et al., 2017), which can complicate interpretation. Head motion can systematically bias estimates of structural connectivity (Baum et al., 2018), and thus we undertook a rigorous protocol to ensure data quality (see Methods: Imaging Data Preprocessing). However, despite assuring maximum reliability of structural connectivity estimates, we must acknowledge that subjects with worse head motion might comprise an important population to which our results may not

generalize. Despite these limitations common to nearly all network analysis of DTI, numerous DTI-based studies of neuropsychiatric illness have described differences in structural brain networks consistent with clinical and neuroscientific priors (Kubicki et al., 2007; Pievani et al., 2011), suggesting that quality-controlled DTI is capable of capturing subtle but meaningful variation in structural connectivity.

It is also important to acknowledge that our analysis of sex differences focuses on sex assigned at birth, which we refer to as "sex" throughout this paper. Our data does not include endocrinological measurements relevant to sex, nor does it include any psychosocial assessment of gender identity. Thus, we were not able to control for or assess gender-based differences in brain structure. Furthermore, while there exist two distinct classes of human genitalia, this fact does not imply that brains are also sexually dimorphic (Joel et al., 2015). Both "male" and "female" features exist in both male and female brains, although some features are more common in one sex than the other (Joel et al., 2015; Joel and McCarthy, 2017). As a result, there may be more meaningful variance in neurologic phenotypes within each sex than between sexes. The divergent controllability-activation profiles in Fig. 8d may be in part due to this fact. Nevertheless, biological sex is an easily measured variable and identifying correlates of sex makes it a useful biomarker. In the future, identification of additional covariates might help uncover a more ubiquitous reason for sex-associated brain features (Joel and McCarthy, 2017).

#### 5. Conclusion

First and foremost, our analysis of sex differences in structural brain networks showed that males and females are highly similar from the perspective of network controllability. The organization of relative controller strength was almost identical between males and females, and sex was not significantly associated with controllability values at most brain regions. However, the differences in average and modal controllability between males and females predicted differences in cognitive performance and effects were most robust in frontal and parietal regions. Given that BOLD signal is associated with network controllability, an interesting future study might use time-invariant, linear dynamics to predict changes in brain activity after stimulation of regions with high versus low controllability. Additionally, our results pave the way for a future study to consider how sex and age may influence the effects of diffusion imaging-guided brain stimulation. Such an approach may help clinicians tune parameters for stimulation a priori based on sex and age, aiding the delivery of personalized psychiatric care.

#### Acknowledgments

This work was supported by an administrative supplement to NIH R21-M MH-106799 (Satterthwaite/Bassett MPI). DSB also acknowledges support from the John D. and Catherine T. MacArthur Foundation, the Alfred P. Sloan Foundation, the Army Research Office through contract number W911NF-14-1-0679, the Army Research Laboratory through contract number W911NF-10-2-0022, the National Institute of Health (2-R01-DC-009209-11, 1R01HD086888-01, R01-MH107235, MH107703, R01MH109520, 1R01NS099348 and R21-M MH-106799), the Office of Naval Research, and the National Science Foundation (BCS-1441502, CAREER PHY-1554488, BCS-1631550, and CNS-1626008). TDS was supported by R01MH107703. DRR was supported by K01MH102609. FP acknowledges support from NSF-BCS-1631112 and NSF-BCS-1430279. The content is solely the responsibility of the authors and does not necessarily represent the official views of any of the funding agencies.

#### Appendix A. Supplementary data

Supplementary data to this article can be found online at https://doi. org/10.1016/j.neuroimage.2018.11.048.

#### References

```
Anderson, V.A., Anderson, P., Northam, E., Jacobs, R., Catroppa, C., 2001. Dev.
    Neuropsychol. 20, 385.
```

Andersson, J.L.R., Sotiropoulos, S.N., 2016. Neuroimage 125, 1063.

Barkley, R.A., Murphy, K.R., Dupaul, G.J., Bush, T., 2002, J. Int. Neuropsychol, Soc. 8,

Baron, R.M., Kenny, D.A., 1986. J. Pers. Soc. Psychol. 51, 1173.

Bassett, D.S., Bullmore, E.T., 2017. Neuroscientist 23, 499.

Baum, G.L., Ciric, R., Roalf, D.R., Betzel, R.F., Moore, T.M., Shinohara, R.T., Kahn, A.E., Vandekar, S.N., Rupert, P.E., Quarmley, M., Cook, P.A., Elliott, M.A., Ruparel, K., Gur, R.E., Gur, R.C., Bassett, D.S., Satterthwaite, T.D., 2017, Curr, Biol, 27, 1561.

Baum, G.L., Roalf, D.R., Cook, P.A., Ciric, R., Rosen, A.F., Xia, C., Elliott, M.A.,

Ruparel, K., Verma, R., Tunç, B., et al., 2018. Neuroimage 173, 275. Bechara, A., Van Der Linden, M., 2005. Curr. Opin. Neurol. 18, 734.

Benjamini, Y., Hochberg, Y., 1995. J. Roy. Stat. Soc. B 289.

Betzel, R.F., Gu, S., Medaglia, J.D., Pasqualetti, F., Bassett, D.S., 2016. Sci. Rep. 6, 30770. Biederman, J., Petty, C.R., Fried, R., Doyle, A.E., Spencer, T., Seidman, L.J., Gross, L., Poetzl, K., Faraone, S.V., 2007. Acta Psychiatr. Scand. 116, 129.

Boes, A.D., Bechara, A., Tranel, D., Anderson, S.W., Richman, L., Nopoulos, P., 2008. Soc. Cognit. Affect Neurosci. 4, 1.

Breheny, P., Burchett, W., 2013. R package 1.

Brewer, J.A., Potenza, M.N., 2008, Biochem, Pharmacol, 75, 63,

Brower, M.C., Price, B., 2001. J. Neurol. Neurosurg. Psychiatr. 71, 720.

Cammoun, L., Gigandet, X., Meskaldji, D., Thiran, J.P., Sporns, O., Do, K.Q., Maeder, P., Meuli, R., Hagmann, P., 2012. J. Neurosci. Methods 203, 386.

Castellanos F.X. Tannock R. 2002 Nat Rev Neurosci 3, 617

Chapple, C.L., Johnson, K.A., 2007. Youth Violence Juv. Justice 5, 221. https://doi.org/ 10.1177/1541204007301286.

Chen, Y., Tymofiyeva, O., Hess, C.P., Xu, D., 2015. Neuroimage 109, 160.

Cornblath, E.J., Ashourvan, A., Kim, J.Z., Betzel, R.F., Ciric, R., Baum, G.L., He, X., Ruparel, K., Moore, T.M., Gur, R.C., et al., 2018. arXiv preprint arXiv:1809.02849.

Coron, J.-M., 2009. Control and Nonlinearity. American Mathematical Society. Cross, C.P., Copping, L.T., Campbell, A., 2011. Psychol. Bull. 137, 97.

Cuadra, M.B., Pollo, C., Bardera, A., Cuisenaire, O., Villemure, J.-G., Thiran, J.-P., 2004. IEEE Trans. Med. Imag. 23, 1301.

Deco, G., Jirsa, V.K., McIntosh, A.R., 2011. Nat. Rev. Neurosci. 12, 43.

Diamond, A., 2013. Annu. Rev. Psychol. 64, 135.

Eriksson, J., Vogel, E.K., Lansner, A., Bergström, F., Nyberg, L., 2015. Neuron 88, 33. Euston, D.R., Gruber, A.J., McNaughton, B.L., 2012. Neuron 76, 1057.

Fair, D.A., Cohen, A.L., Power, J.D., Dosenbach, N.U., Church, J.A., Miezin, F.M., Schlaggar, B.L., Petersen, S.E., 2009. PLoS Comput. Biol. 5, e1000381. Fischl, B., 2012. Neuroimage 62, 774.

J. Fox, S. Weisberg, D. Adler, D. Bates, G. Baud-Bovy, S. Ellison, D. Firth, M. Friendly, G. Gorjanc, S. Graves, et al., Vienna: R Foundation for Statistical Computing (2012).

Galan, R.F., Ermentrout, G.B., Urban, N.N., 2008. J. Neurophysiol. 99, 27 Gennatas, E.D., Avants, B.B., Wolf, D.H., Satterthwaite, T.D., Ruparel, K., Ciric, R., Hakonarson, H., Gur, R.E., Gur, R.C., 2017. J. Neurosci. https://doi.org/10.1523/ JNEUROSCI.3550-16.2017.

Giedd, J.N., Blumenthal, J., Jeffries, N.O., Castellanos, F.X., Liu, H., Zijdenbos, A., Paus, T., Evans, A.C., Rapoport, J.L., 1999. Nat. Neurosci. 2, 861.

Gogtay, N., Giedd, J.N., Lusk, L., Hayashi, K.M., Greenstein, D., Vaituzis, A.C., Nugent, T. F. r., Herman, D.H., Clasen, L.S., Toga, A.W., Rapoport, J.L., Thompson, P.M., 2004. Proc. Natl. Acad. Sci. U. S. A. 101, 8174.

Goldstein, J.M., Jerram, M., Poldrack, R., Anagnoson, R., Breiter, H.C., Makris, N., Goodman, J.M., Tsuang, M.T., Seidman, L.J., 2005. Neuropsychology 19, 509.

Greve, D.N., Fischl, B., 2009. Neuroimage 48, 63.

Gu, S., Pasqualetti, F., Cieslak, M., Telesford, Q.K., Alfred, B.Y., Kahn, A.E., Medaglia, J.D., Vettel, J.M., Miller, M.B., Grafton, S.T., et al., 2015. Nat. Commun. 6. Gu, S., Betzel, R.F., Mattar, M.G., Cieslak, M., Delio, P.R., Grafton, S.T., Pasqualetti, F.,

Bassett, D.S., 2017. Neuroimage 148, 305. Gu, S., Cieslak, M., Baird, B., Muldoon, S.F., Grafton, S.T., Pasqualetti, F., Bassett, D.S., 2018. Sci. Rep. 8, 2507.

Gur, R.C., Richard, J., Hughett, P., Calkins, M.E., Macy, L., Bilker, W.B., Brensinger, C., Gur, R.E., 2010. J. Neurosci. Methods 187, 254.

Gur, R.C., Richard, J., Calkins, M.E., Chiavacci, R., Hansen, J.A., Bilker, W.B., Loughead, J., Connolly, J.J., Qiu, H., Mentch, F.D., et al., 2012. Neuropsychology 26,

Hasson, R., Fine, J.G., 2012. J. Atten. Disord. 16, 190.

Heatherton, T.F., Wagner, D.D., 2011. Trends Cognit. Sci. 15, 132.

Honey, C., Sporns, O., Cammoun, L., Gigandet, X., Thiran, J.-P., Meuli, R., Hagmann, P., 2009. Proc. Natl. Acad. Sci. Unit. States Am. 106, 2035.

Horn, N., Dolan, M., Elliott, R., Deakin, J., Woodruff, P., 2003. Neuropsychologia 41,

Hosenbocus, S., Chahal, R., 2012. J. Can. Acad. Child Adolesc. Psychiatr. 21, 223. Hyde, J.S., 2014. Annu. Rev. Psychol. 65, 373.

Ingalhalikar, M., Smith, A., Parker, D., Satterthwaite, T.D., Elliott, M.A., Ruparel, K., Hakonarson, H., Gur, R.E., Gur, R.C., Verma, R., 2014. Proc. Natl. Acad. Sci. Unit. States Am. 111, 823. http://www.pnas.org/content/111/2/823.full.pdf.

Izhikevich, E.M., Edelman, G.M., 2008. Proc. Natl. Acad. Sci. Unit. States Am. 105, 3593. Jeganathan, J., Perry, A., Bassett, D.S., Roberts, G., Mitchell, P.B., Breakspear, M., 2018. Neuroimage: Clin. 19, 71.

Jenkinson, M., Bannister, P., Brady, M., Smith, S., 2002. Neuroimage 17, 825. Jenkinson, M., Beckmann, C.F., Behrens, T.E., Woolrich, M.W., Smith, S.M., 2012. Neuroimage 62, 782.

Joel, D., 2012. Biol. Sex Differ. 3, 27.

- Joel, D., McCarthy, M.M., 2017. Neuropsychopharmacology 42, 379.
- Joel, D., Berman, Z., Tavor, I., Wexler, N., Gaber, O., Stein, Y., Shefi, N., Pool, J., Urchs, S., Margulies, D.S., et al., 2015. Proc. Natl. Acad. Sci. Unit. States Am. 112, 15468.
  Jones, D.K., Basser, P.J., 2004. Magn. Reson. Med. 52, 979.
- Kailath, T., 1980. Linear Systems. Prentice Hall, Englewood Cliffs.
- Kalman, R.E., Ho, Y.C., Narendra, K.S., 1963. Contrib. Differ. Equ. 1, 189.
- Keulers, E.H., Stiers, P., Jolles, J., 2011. Neuroimage 54, 1442.
- Kim, J., Soffer, J.M., Kahn, A.E., Vettel, J.M., Pasqualetti, F., Bassett, D.S., 2018. Nat. Phys. 14, 91.
- Koenigs, M., Barbey, A.K., Postle, B.R., Grafman, J., 2009. J. Neurosci. 29, 14980. Kubicki, 1M., McCarley, R., Westin, C.-F., Park, H.-J., Maier, S., Kikinis, R., Jolesz, F.A., Shenton, M.E., 2007. J. Psychiatr. Res. 41, 15.
- Leith, D.J., Leithead, W.E., 2000. Int. J. Contr. 73, 1001.
- Lenroot, R.K., Gogtay, N., Greenstein, D.K., Wells, E.M., Wallace, G.L., Clasen, L.S., Blumenthal, J.D., Lerch, J., Zijdenbos, A.P., Evans, A.C., et al., 2007. Neuroimage 36, 1065.
- Li, C.-s. R., Luo, X., Yan, P., Bergquist, K., Sinha, R., 2009. Alcohol Clin. Exp. Res. 33, 740. Liu, Y.Y., Slotine, J.J., Barabasi, A.L., 2011. Nature 473, 167.
- Maier-Hein, K.H., Neher, P.F., Houde, J.-C., Côté, M.-A., Garyfallidis, E., Zhong, J., Chamberland, M., Yeh, F.-C., Lin, Y.-C., Ji, Q., et al., 2017. Nat. Commun. 8, 1349. Miller, D.I., Halpern, D.F., 2014. Trends Cognit. Sci. 18, 37.
- Motter, A.E., 2015. Chaos 25, 097621.
- Muldoon, S.F., Pasqualetti, F., Gu, S., Cieslak, M., Grafton, S.T., Vettel, J.M., Bassett, D.S., 2016. PLoS Comput. Biol. 12, e1005076.
- Murphy, A.C., Bassett, D.S., 2017. Curr. Opin. Biomed. Eng. 1, 63.
- Nomi, J.S., Bolt, T.S., Ezie, C.E.C., Uddin, L.Q., Heller, A.S., 2017. J. Neurosci. 37, 5539. Obrien, R.M., 2007. Qual. Quantity 41, 673.
- Pasqualetti, F., Zampieri, S., Bullo, F., 2014. IEEE Trans. Contr. Net. Syst. 1, 40. Pecora, L.M., Carroll, T.L., 1998. Phys. Rev. Lett. 80, 2109.
- Pievani, M., de Haan, W., Wu, T., Seeley, W.W., Frisoni, G.B., 2011. Lancet Neurol. 10, 829
- Pohjalainen, T., Rinne, J.O., Någren, K., Syvälahti, E., Hietala, J., 1998. Am. J. Psychiatr. 155, 768.
- Preacher, K., Curran, P., Bauer, D., 2004. Simple Intercepts, Simple Slopes, and Regions of Significance in Mlr 2-way Interactions.
- R Core Team, R., 2017. A Language and Environment for Statistical Computing. R Foundation for Statistical Computing, Vienna, Austria.
- Ragland, J.D., Turetsky, B.I., Gur, R.C., Gunning-Dixon, F., Turner, T., Schroeder, L., Chan, R., Gur, R.E., 2002. Neuropsychology 16, 370.
- Raichle, M.E., 2015. Annu. Rev. Neurosci. 38, 433.
- Riley, E., Okabe, H., Germine, L., Wilmer, J., Esterman, M., DeGutis, J., 2016. PLoS One 11, e0165100.

- Roalf, D.R., Quarmley, M., Elliott, M.A., Satterthwaite, T.D., Vandekar, S.N., Ruparel, K., Gennatas, E.D., Calkins, M.E., Moore, T.M., Hopson, R., et al., 2016. Neuroimage 125, 903. Romer, D., Betancourt, L., Giannetta, J.M., Brodsky, N.L., Farah, M., Hurt, H., 2009. Neuropsychologia 47, 2916.
- Rosen, A.F., Roalf, D.R., Ruparel, K., Blake, J., Seelaus, K., Villa, L.P., Ciric, R., Cook, P.A., Davatzikos, C., Elliott, M.A., et al., 2018. Neuroimage 169, 407
- Satterthwaite, T.D., Wolf, D.H., Erus, G., Ruparel, K., Elliott, M.A., Gennatas, E.D., Hopson, R., Jackson, C., Prabhakaran, K., Bilker, W.B., et al., 2013. J. Neurosci. 33, 16249.
- Satterthwaite, T.D., Wolf, D.H., Roalf, D.R., Ruparel, K., Erus, G., Vandekar, S., Gennatas, E.D., Elliott, M.A., Smith, A., Hakonarson, H., et al., 2014. Cerebr. Cortex 25, 2383
- Satterthwaite, T.D., Elliott, M.A., Ruparel, K., Loughead, J., Prabhakaran, K., Calkins, M.E., Hopson, R., Jackson, C., Keefe, J., Riley, M., Mentch, F.D., Sleiman, P., Verma, R., Davatzikos, C., Hakonarson, H., Gur, R.C., Gur, R.E., 2014. Neuroimage 86, 544.
- Schmithorst, V.J., Vannest, J., Lee, G., Hernandez-Garcia, L., Plante, E., Rajagopal, A., Holland, S.K., Consortium, C.A., 2015. Hum. Brain Mapp. 36, 1.
- Shanmugan, S., Wolf, D.H., Calkins, M.E., Moore, T.M., Ruparel, K., Hopson, R.D., Vandekar, S.N., Roalf, D.R., Elliott, M.A., Jackson, C., et al., 2016. Am. J. Psychiatry 173, 517
- Snodgrass, J.G., Corwin, J., 1988. J. Exp. Psychol. Gen. 117, 34.
- Sobel, M.E., 1982. Socio. Methodol. 13, 290.
- Stephan, K., Schlagenhauf, F., Huys, Q., Raman, S., Aponte, E., Brodersen, K., Rigoux, L., Moran, R., Daunizeau, J., Dolan, R., Friston, K., Heinz, A., 2017. Neuroimage 145, 180 (individual Subject Prediction).
- Straube, T., Schmidt, S., Weiss, T., Mentzel, H.-J., Miltner, W.H., 2009. Hum. Brain Mapp. 30, 689.
- Tang, E., Giusti, C., Baum, G.L., Gu, S., Pollock, E., Kahn, A.E., Roalf, D.R., Moore, T.M., Ruparel, K., Gur, R.C., Gur, R.E., Satterthwaite, T.D., Bassett, D.S., 2017. Nat. Commun. 8, 1252.
- Tanji, J., Hoshi, E., 2008. Physiol. Rev. 88, 37.
- Vandekar, S.N., Shinohara, R.T., Raznahan, A., Roalf, D.R., Ross, M., DeLeo, N., Ruparel, K., Verma, R., Wolf, D.H., Gur, R.C., et al., 2015. J. Neurosci. 35, 599. Wang, B., 2018. R package 1.
- Weafer, J., de Wit, H., 2014. Addict. Behav. 39, 1573.
- Whalen, A.J., Brennan, S.N., Sauer, T.D., Schiff, S.J., 2015. Phys. Rev. X 5, 011005.
   Wiles, L., Gu, S., Pasqualetti, F., Bassett, D.S., Meaney, D.F., 2017. Scientific Reports in Press.
- Wu-Yan, E., Betzel, R.F., Tang, E., Gu, S., Pasqualetti, F., Bassett, D.S., 2018. J. Nonlinear Sci. 1.
- Zhu, T., Hu, R., Qiu, X., Taylor, M., Tso, Y., Yiannoutsos, C., Navia, B., Mori, S., Ekholm, S., Schifitto, G., et al., 2011, Neuroimage 56, 1398.